CrossMark

Combining series of multi-source high spatial resolution remote sensing datasets for the detection of shoreline displacement rates and the effectiveness of coastal zone protection measures

A. Tsokos[1] · E. Kotsi[2] · S. Petrakis[2] · Emm Vassilakis[2]

Abstract

The long-term change of the shoreline location is a phenomenon, which is highly factored in the design of construction projects along the coastal zone. Especially, beach erosion is characterized as one of the major problems at coastal areas and it is of high importance as a quite significant percentage of social development is concentrated in a relatively narrow zone not far from the waterfront. This study presents a methodology that aims to quantify the shoreline displacement rate by involving the processing of different types of remote sensing datasets such as aerial photographs, satellite images and unmanned aerial system data coupled with in-situ observations and measurements. Several photogrammetric techniques were used in order to orthorectify and homogenize a time series of remotely sensed data acquired from 1945 to 2017, representing a rapidly relocating coastal zone at the southern part of Corinth Gulf (Greece), as a case study. All images were digitally processed and optically optimized in order to produce a highly accurate representation of the shoreline at the time period of each acquisition. The data were imported in a Geographic Information System platform, where they were subjected to comparison and geostatistical analysis. High erosion rates were calculated, reaching the order of 0.18 m/year on average whilst extreme rates of 0.70 m/year were also observed in specific locations leading to the segmentation of the coastal zone according to its vulnerability and consequently the risk for further development as well as the effectiveness of measures already taken by the authorities.

Keywords Ikonos-2 · Worldview-2 · UAS · Photogrammetry · DSAS · Corinth gulf

Introduction

The radical displacement of the shoreline during time is one of the most important factors to be taken under consideration when designing infrastructures along the coastal zones (De Pippo et al. 2008; Anthoff et al. 2010; Nicholls and Hoozemans 1996). Given that a large number of human activities take place near or along the coastline (Costanza et al. 1997), it is important to point out the high-risk areas and quantify any potential erosion with the highest possible accuracy (Evans et al. 2004). Serious changes in the topography along the shoreline, as well as severe erosion phenomena have been recorded in large areas due to human presence and activities (Kloehn et al. 2008; Van Rijn 1998). The study of these changes during the last decades can provide the scientists with a chance to calculate the rate of shoreline displacement using various methods (Van Zuidam and Van Zuidam-Cancelado 1979; Alhin and Niemeyer 2009). In order to estimate this rate of evolution, a long-time series of data going back in time is needed (Malthus and Mumby 2003; Boak and Turner 2005). These data usually involve remotely sensed observations, such as aerial photographs or digital satellite images. Digital processing of the aforementioned data, combined with in-situ measurements can provide important information during the acquisition period. The process of digital

✉ Emm Vassilakis
evasilak@geol.uoa.gr

A. Tsokos
atsokos@gmail.com

E. Kotsi
ekotsi@gmail.com

S. Petrakis
spetrakis@geol.uoa.gr

1 Department of Civil Engineering, Laboratory of Harbor Works (LHW), National Technical University of Athens, Athens, Greece

2 Faculty of Geology and Geoenvironment, National & Kapodistrian University of Athens, 15784 Athens, Greece

🙂 Springer

interpretation of such data is of utmost importance so as to create ortho-corrected datasets for each time period and results in the derivation of comparable data and implications for the environmental impact of the phenomena (Vassilakis 2010). The processing of the historical data can also be compared to data acquired by Unmanned Aerial Systems (UAS) showing the contemporary state of the shoreline and such flights could provide a denser timeseries for the future observations of any study area. Moreover, the collection of field data and their validation is important in order to specify the real causes of the changes in the shoreline, which can be related to physical processes, human activity or both (Valaouris et al. 2014).

Study area

The area of interest is situated at the southern shoreline of the Corinth Gulf in Greece, where the beach zones are under significant neotectonic control. A large number of active fault zones hosting significant and in many cases catastrophic earthquake events (Fig. 1a), develop subparallel to the current shoreline and contribute to the constant widening of the gulf (e.g. Sakellariou et al. 2007; Bell et al. 2009; Charalampakis et al. 2014; Albini et al. 2017). The widening happens along NNW-SSE direction and the rate of displacement is of the order of 14 mm/year according to GPS measurements (McClusky et al. 2000; Hollenstein et al. 2008; Vassilakis et al. 2011). This phenomenon has a direct impact on the displacement of the shoreline position. The severe changes in the position of the shoreline in the long term are one of the most important issues due to hazard assessment at the selected area of the Gulf of Corinth (Fig. 1b).

The Corinth Gulf area is characterized as micro-tidal, since the combination of astronomical and meteorological tides is relatively low (Evelpidou et al. 2011). The recently published report of the Hellenic Navy Hydrographic Service (HNHS 2015) mentions that the Mean High Water is 0.89 m, for the period between 1990 and 2012. The orientation of the area (NW-SE) protects the beach from the strong westerly winds and thus prevents the sea surface elevation rise caused by the corresponding waves. Furthermore, sea level rise due to eustatism for the past 72 years is below 30 cm in total (Church et al. 2013), which doesn't affect significantly the essence of this study.

A quite high number of either small or larger river mouths are located along the entire area of the southern coastline of the Gulf of Corinth, feeding it up with large quantities of eroded material since Pleistocene. The deposited beds at the estuaries are usually found tilted towards upstream (Vassilakis et al. 2007). The result of the tectonic movements is the continuous uplifting of the northern beaches of Peloponnesus and consequently intensive incision and erosion in depth leading to the development of canyons trending normal to the coastal zone. This, in turn, contributes to the constant input of sediment in the deltaic

areas. In that sense, alluvium and contemporary material transported through rivers consisting of coarse material like sand and breccia can be found along the shoreline. Some berms of small thickness have also been observed in specific areas.

The morphological slopes along the beach zone are mild with values of up to 5%. The in-situ measurements verify the mild slopes and the lack of scarps, at least in the area described in this paper. The underwater morphology is also affected by the same geodynamic processes expressed as failures and geomorphic features that indicate underwater instabilities probably triggered, directly or indirectly, by the ongoing active tectonic deformation. Several studies have proved that the entire southern margin of the Corinth Rift is characterized by intense relief and a narrow, almost absent, continental shelf, which passes abruptly to steep submarine slopes (Lykousis et al. 2007; Nomikou et al. 2011). These high slope angles are related to submarine instabilities and failures which in turn - along with the seafloor currents- affect the coastal zone causing shoreline displacement.

The area selected for the application of the specific methodology is a very characteristic segment of the Corinth Gulf and has an overall length of 12 km. It lies between the Town of Sykea (east) and the Town of Kamari (west) including the entire waterfront of the Town of Xilokastro, where large residential and tourist development has occurred during the last decades. The local authorities keep spending great amount of money into constructing various works along the shoreline for the protection of the beachfronts from erosion but without significant results, so far other than slowing down the phenomenon.

Data and methods

The methodology described in this study was based on using three different types of remote sensing data. Historical analogue panchromatic aerial images of high resolution (Van Zuidam and Van Zuidam-Cancelado 1979), recent digital high resolution multi-spectral satellite as well as contemporary ortho-photo-mosaic derived from photographs acquired with the use of UAS were used for extracting with high detail the exact location of the shoreline during each acquisition time period. The acquisition of the aerial photographs took place during 1945, 1987, 1996 and 2010, the satellite images where acquired during 2000, 2008 and 2012 and the UAS flight was scheduled at June 2017 (Fig. 2). A time dependent analysis was conducted aiming to identify and quantify the coastal retreat or progradation throughout the selected time period by using geo-informatics methodologies and tools in a Geographic Information System (GIS) environment. Nearshore bathymetric profiles were also used in order to study how the underwater morphology affects the coastline displacement.
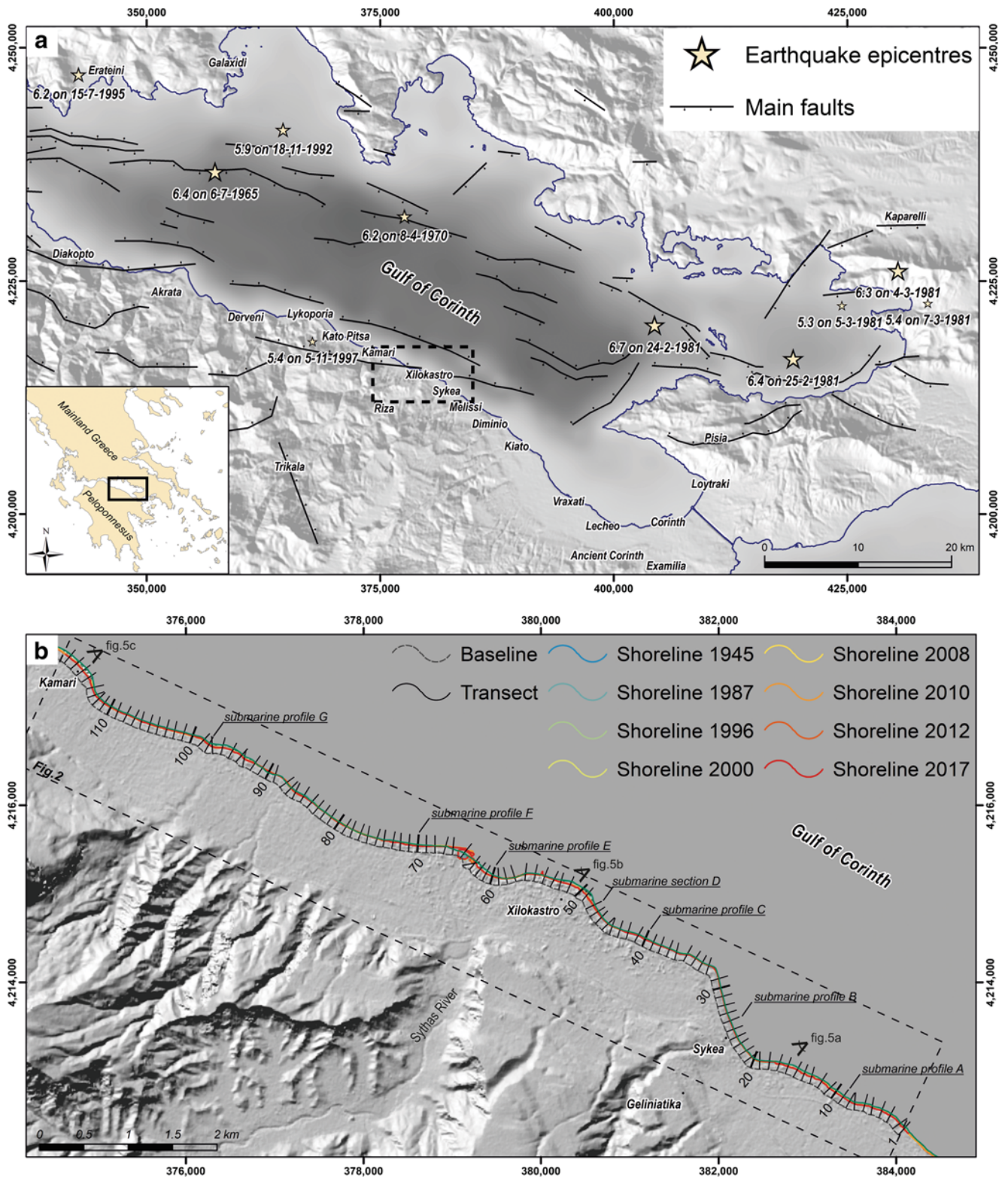
Fig. 1 a Index map of the Corinth Gulf and the location of the epicentres of the most significant seismic events for the study period, as well as the main fault traces. The inset shows the exact location of the Corinth Gulf in Greece and the dashed rectangle shows the magnified area of interest below. **b** The topography of the Corinth Gulf coastal zone segment on which the described methodology was applied. The shoreline traces for each time period are presented, as well as the location of the 118 transects and the baseline which was used for calculating the shoreline displacement. Additionally, the seven submarine profiles conducted across the coastline at selected coastal segments are shown. The dashed rectangle represents the area covered by the remote sensing data in Fig. 2, whilst the locations of the photographs of Fig. 5 are also noted
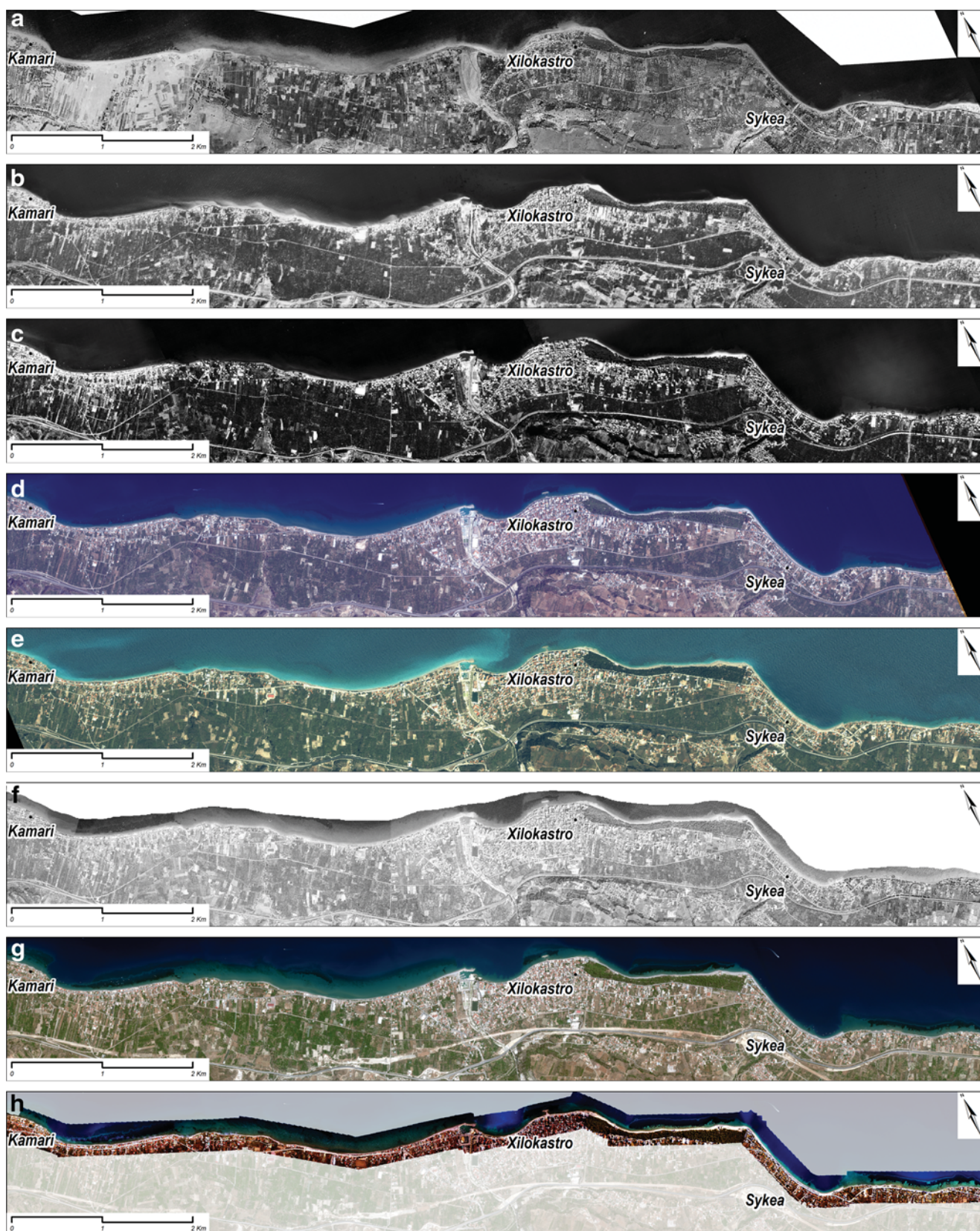
Fig. 2 The remote sensing data used for this study covering a time lapse of 72 years (1945–2017) and a twelve kilometers coastal zone at the southern margin of Corinth Gulf between the places of Kamari - Xilokastro - Sykia. Historical aerial photographs from 1945 (**a**), 1987 (**b**), 1996 (**c**), 2010 (**f**); satellite images from 2000 (**d**, Ikonos-2 / Aug 24th), 2008 (**e**, Ikonos-2 / Apr 24th), 2012 (**f**, WorldView-2 / Jul 28th); UAS aerial photographs from 2017 / Jun 20th (**h**) have been orthorectified and referenced into GGRS'87 projection system in order to be comparable. Changes regarding the shoreline as well as the land are rather observable with bare eyes

Historical analog aerial photographs

The panchromatic aerial photographs were collected from several local agencies scanned with a large format scanner high-resolution scanner (1200 dpi) (Chaaban et al. 2012) and were ortho-rectified using photogrammetric software (Vassilakis and Papadopoulou-Vrynioti 2014). During the ortho-rectification procedure of the scanned aerial photographs, a high resolution digital elevation model was used as an elevation reference. The latter reached the spatial resolution of 5 m and was created by the Greek National Cadastre & Mapping Agency S.A. (NCMA S.A.) with photogrammetric methods. As a reference dataset we used the 2010 ortho photo mosaic constructed also by NCMA S.A. (Fig. 2f). This procedure led to the production of three more panchromatic ortho photo mosaics with spatial resolution of 1 m, one for each year of observation (1945, 1987, and 1996) (Fig. 2a, b and c respectively) showing the coastline location during the acquisition time (Moore 2000).

Satellite images

In a similar manner, high resolution satellite images were ortho-rectified to create three multi-spectral images for the periods of 2000, 2008 and 2012 (Fig. 2d, e and g respectively). The satellite images which were used in this work were Ikonos-2 (for the years 2000 and 2008) with spatial resolution of 1 m and Worldview-2 (for the year 2012) with spatial resolution of 0.5 m after resolution merging. The datasets were pre-processed before the ortho-rectification procedure including pan-sharpening for increasing the spatial resolution by using the Hyperspherical Color sharpening algorithm (Padwick et al. 2010) which is specially designed for the WorldView-2 sensor multi-band data and seems to work efficiently with other multispectral data containing more than 3 bands such as Ikonos-2. According to the workflow of this algorithm the imagery data are transformed from native color space to hyperspherical color space, in order to replace the multispectral intensity component with an intensity matched version of the panchromatic band for each dataset. The ortho-rectification procedure was based on the 2010 reference dataset and the NCMA digital elevation model as well.

Unmanned aerial system aerial photographs

The contemporary location of the studied segment of the coastline was extracted with the implementation of a rotor-wing UAS (DJI Phantom 3 Advanced drone) during a field survey. It was used in order to collect high resolution natural colour images with its built-in camera (with 3.61 mm focal length) bundled on a two-axis gimbal. Nine surveys were conducted for covering a total length of 12 km of the coastal zone and a total area of about 4 km^2. Each survey was programmed at a flight elevation of 120 m above the take off point (located on the beach) and lasted approximately 15 min. The image acquisition survey was designed to cover the study area in a two-way flight along the coastal zone with high resolution, overlapping, natural colour photographs. In order to obtain a satisfying overlap (70% front lap and side lap) during the image acquisition, the flight height and the density of the images had to be taken under consideration, not to forget the battery usage limitations. The percentage of overlapping is quite crucial as it had to be high enough for a successive photogrammetric interpretation and ortho photo mosaic construction without any artefacts, at a later stage. The UAS platform is equipped with a GPS antenna which provides quite good precision especially for the horizontal axis the measurements of which are also used for the alignment of the images captured during the survey (Fonstad et al. 2013).

A total of 478 images (4000 × 3000 pixels each) was acquired with 70% overlapping and after aligning them a sparse 3D point cloud representing the most prominent features in the images was produced (Fig. 2h). Image processing followed the recommended procedure outlined by Agisoft (2016) which was slightly modified for reducing geometry errors and constructing a dense point cloud. The latter consisted of more than 620 million points covering the entire length of the coastal zone. The information for each point of them includes values of reflectance at the visible (BGR) spectra along with X, Y, Z coordinates, which were calculated after taking into account the positions of the camera when shooting at each point from different angles (Westoby et al. 2012). The procedure continued with meshing the original images as fine topographic details were available. Texturing was also applied to the resulted mesh in a later step and an ortho-image was generated (Mancini et al. 2013).

Shoreline displacement analysis

The geometrically corrected data were projected in the same reference system through the ortho rectification procedure, covering a total time period of 72 years. At all stages of the described methodology the Greek Geodetic Reference System of 1987 (GGRS '87) was used (Mugnier 2002). Therefore, by using image processing techniques for interpreting and enhancing all images, the shoreline for each one of the aforementioned datasets had to be digitized and imported into a

geographic information platform in order to be comparable and reliable as far as its displacement through time. The most critical and time-consuming part of the methodology was to identify with high accuracy the separation points between the waterbody and the land. In order to accurately project the shoreline, the histogram of each image was equalized and in some cases a weight coefficient was used. The latter varies for each aerial photograph, taking into account the details of the flight and the relative position of the sun. As far as working with the satellite images, digitizing the shoreline was rather effortless since the infrared band was included in the provided datasets. Since this part of the electro-magnetic spectrum is almost entirely absorbed by clear waterbodies (Gens 2010), it was pretty easy to extract the shoreline providing uniformity and objectivity in the methodology. The latter is a significant feature of the present study as the implementation of a methodology capable of providing comparable results is of high importance.

In a way to achieve this, an extension of the ESRI ArcGIS v.10 software was employed as published by USGS and named Digital Shoreline Analysis System v.4.3 (DSAS). The DSAS extension (Thieler et al. 2009) lets the user define a constant straight line in a specific distance from the shoreline and take transects perpendicular to it among the evolving coastlines (Fig. 1). The measurements give quantitative information on the change of the position of the shoreline, as well as more useful statistical data. The distance between the transects was set at every 100 m. Even if this seems to be an arbitrary value, it worked rather sufficiently at this almost 12 km long segment of the shoreline as it can be characterized as rather curvy and either a smaller value would result an oversampled area with transects intersect each other mixing the calculations or a larger value would result quite sparse transect locations without any representative outcome.

A total number of 118 transects were created covering a waterfront segment of 11.9 km, in order to estimate the evolution of the shoreline and quantify the rate of displacement between 1945 and 2017. For each transect eight measurements were conducted, one for each time period regarding the absolute distance between every digitized shoreline and a given baseline, which was digitized 50 m offshore parallel to the oldest shoreline trace. The distance of the baseline was set to 50 m in order to avoid that an erosional phenomenon would exceed this spacing and consequently intersect with any of the digitized shorelines.

The outcome of this procedure is a spatially joined table containing several measurements and calculations referring to each one of the transects describing the area immediately seaward of the current shoreline (Thieler et al. 2009). The table containing the statistical data can be used either to produce graphs (Fig. 3) or visualize them in a digital map, in an effort to identify segments of the coastline which suffer significant changes and quantify them as well.

Near shore bathymetry profiles

After a first interpretation of the shoreline timeseries and the preliminary results about the coastal displacement at the studied segment of the Corinth Gulf, a series of near shore profiles were conducted in order to record the bathymetric relief perpendicular to the coast. Seven submarine profiles were created until reaching the depth of about 20 m, with measurements every 4 m (Fig. 4), as it seems that beach erosion might be in some way associated with the near-shore bathymetry, among others. In addition, some of these submarine profiles were compared to previously published profiles at the exact same areas, dated from 2010 (Valaouris et al. 2014), aiming to extract conclusions on the sea-bottom alterations during the last 7 years.

At a first glance, the variation of the subaqueous slopes is obvious since the slope of the nearshore area (up to about 300 m away from the shoreline) varies from an overall of 6.5% (profile F) to 38% (profile B). Usually the relief deepens smoothly towards the 5-m isobath as this is clear at all profiles and it differentiates from that point to increased values, especially at profiles B, D and E. The latter could be rather significant as the reduced distance between the 5-m isobaths and the coastline seem to enhance the erosive ability of the incoming waves especially when the subaerial part consists mostly of sand, with relatively coarser material (gravels, pebbles) on the beach face (Valaouris et al. 2014).

Results and discussion

The outcome of the interpretation regarding the methodology we have described can be rather enlightening about the beach erosion risk of a given study area. By applying geostatistical analysis and thematic mapping techniques in any GIS platform, a color-coding based on the calculated shoreline displacement rate could be easily lead to the identification of segments with retrogradation indications (Fig. 4). On top of this a full quantification record for each one of the 100 m beach segment is attached to a geodatabase, which can be enriched with more field measurements and observations in the future. In this case, we tried to correlate the rate calculations with either ground truth observations and near-shore bathymetric profiles at the most representative segments of the study area (Fig. 4).

One of the most well-defined segment (SG-I, Fig. 3) with coastal erosion rates with an average retreat of 0.30 ± 0.03 m/year, lies at the easternmost part of the study area. This is a mainly residential region of the village Sykea, with land properties that almost reach the shoreline. The coastal erosion is really obvious and during the last two decades several measures have been taken by the local authorities aiming to protect the coastal zone. The main effort was to trap most of the sand
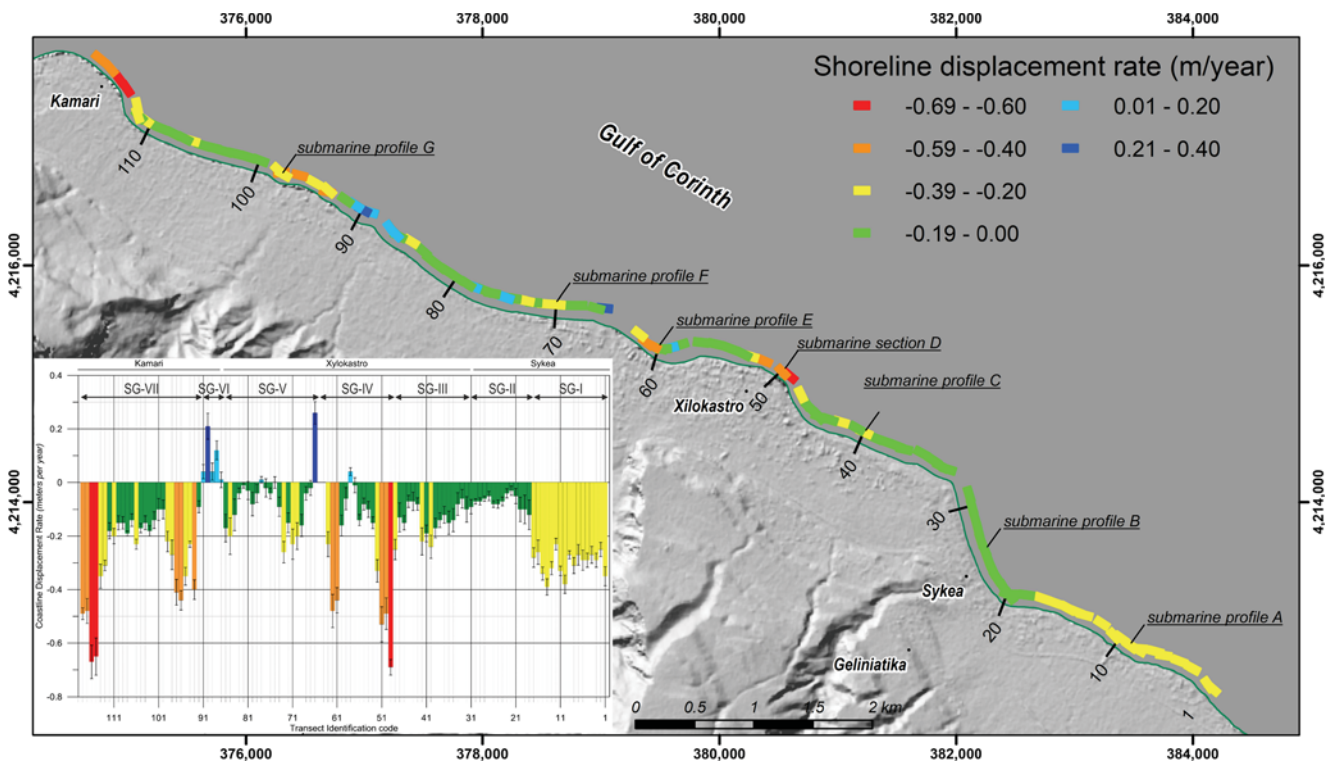
Fig. 3 The geostatistical analysis part of the described methodology led to the spatial distribution of the shoreline displacement rate along the studied area in 100 m long segments. The inset graph represents the displacement rate in higher detail for comparison reasons on which the segments (SG I-VII) mentioned in the text are also placed. The submarine profile locations are also shown for better understanding of this segmentation of the study area in relatively homogenous parts of the coastal zone as discussed in the text

and the relatively coarser material on the beach face around large piers using boulders which would also reduce the erosive ability of the incoming waves. These works seem to somehow decelerate the erosion rate but in any case, an average of nearly 20 m of beach have been vanished along this particular segment -at least for the studied time period of the last 72 years- even though there are transects where the coastal zone has been reduced by even more than 30 m (Fig. 5a). The submarine profile A which was conducted at the location of transect 9, shows a rather smooth subaqueous slope of 10%, reaching the 5-m isobath at nearly 50 m distance from the shoreline. After the isobath of −10, the seabed slope steepens slightly, reaching the isobath of −20 m with a slope of 13%. Even though it steepens more further away from the coastal zone, after about 90 m, there are some anomalies near the shore, maybe regarding to submarine instabilities, which are possibly affecting the shoreline location.

The next segment which is pretty much worth to refer to is a NNW-SSE trending linear shoreline at the waterfront of Sykea village (SG-II, Fig. 3). Most of this segment is under erosion control as a retaining wall has been constructed along the beach, protecting also the main avenue passing through the village as the specific road is the main transportation route in the wider area. Even if the calculated average erosion rate is quite low (0.07 ± 0.02 m/year), it is rather clear that the wall construction which took place during the early 90's is the main cause for it,

preventing severe erosion and serious damage along this part of the coastal zone. The sea bottom profile B was conducted along the transect 26 where almost 6 m of beach have been removed during the last 72 years. It is the steepest relief observed, with an overall slope of 38%, as it reaches the depth of 25 m just 65 m far from the current shoreline. This is an indication that the vulnerability along this segment is increased as well as its risk due to the significance of the wall construction.

Moving westwards towards the town of Xilokastro a 2-km beach segment (SG-III, Fig. 3) lies right in front of a thin pine forest stripe being undisturbed by the human intervention. No constructions have altered the coastal interaction with the wave force as this is clear at all the remote sensing datasets, since 1945 (Fig. 2). The average width of the beach is almost 10 m but we measured that another 12 m consisted of pebbles, gravels and sand have been disappeared the last 72 years. At some transect locations the beach erosion reaches the 20 m but the estimated retrogradation rate is about 0.14 ± 0.03 m/year. The largest local erosion rates were calculated at transects 40 (0.24 ± 0.04 m/year) and 48 (0.25 ± 0.03 m/year). The first one was selected for conducting a submarine profile (C) as its location at the center of this segment seemed to be more representative. The relief of the sea bottom is rather smooth, with an overall slope of about 10%, reaching the 5-m isobath at the distance of 50 m away from the shoreline and exceeding the 200 m for reaching the depth of 20 m. The interpretation of
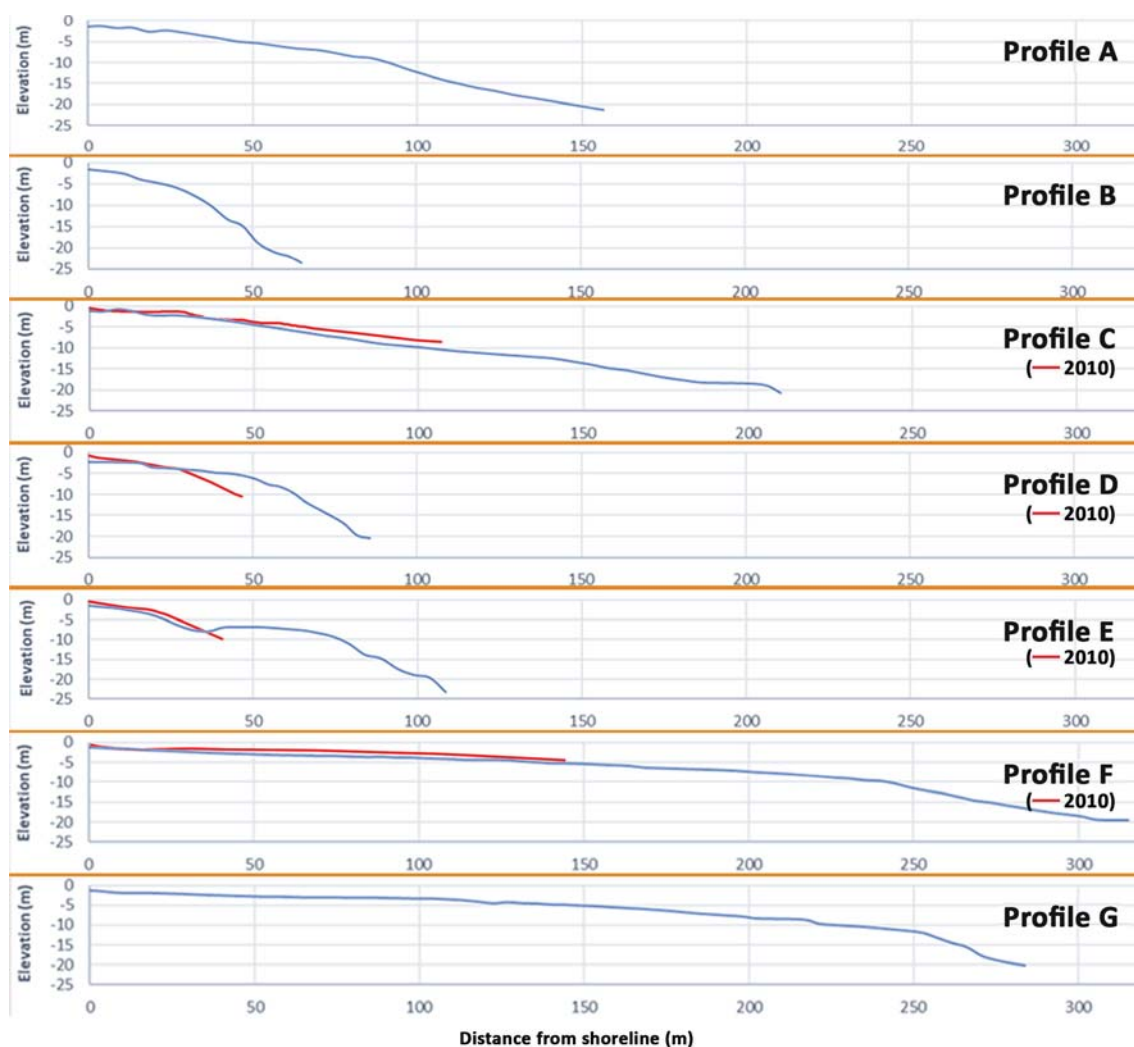
Fig. 4 Seven submarine profiles were conducted, at the end of spring 2017, across the shoreline with sea bottom depth measurements every 4 m. The complexity of the subaqueous relief throughout the study area is rather obvious as smooth slopes co-exist with zones of active instabilities causing steeper irregularities at the sea bottom. The red lines in C, D, E, F profiles represent the sea-bottom relief after measurements during 2010. The relief along the profile D has changed dramatically, in contradiction to profiles C, E and F where the sea-bottom slopes remain relatively unchanged

the bathymetric data shows a slight anomaly at the shallowest 15–20 m as it is clear that the sea bottom rises before it deepens again after a small shelf at the distance of 30 m. The aforementioned underwater morphology was also observed at the drone photographs taken over this location, representing a thin submerged piece of land parallel to the contemporary shoreline. This could be explained as the head of a submarine landslide which may have been triggered by one of the many earthquake events that are hosted at the area of the Corinth Gulf (Nomikou et al. 2011). Comparing the contemporary underwater morphology of this profile with the one from 2010 (Fig. 4), we can conclude that the underwater morphology has not changed significantly, since the small-scale alterations can be justified through the ephemeral changes of the wave regime at the broad area.

The Xilokastro town waterfront develops between transects 49 and 65 (SG-IV, Fig. 3). For more than 1.5 km several constructions have been made and series of measures have been taken in order to preserve the coastal zone and protect from severe erosion phenomena. A retaining wall has been gradually constructed for the protection of the sea side road. The construction of the eastern and western section of the retaining wall was completed during 1969 and 1985, respectively. Later on, the wall was reinforced furthermore by installing natural protective boulders (Fig. 5b). During 1993, breakwater piers were constructed parallel to the seaside in order to create a tombolo by using the large sediment quantities accumulated by Sythas River that bounds the westernmost town's waterfront, but the shoreline along the coastal zone kept receding. The latter was caused either by the eroding action of waves or because the river material transfer has been decreased due to the use of large amounts of river sediments in several constructions. A very significant infrastructure is the Xilokastro yacht marina which has been placed exactly at

Fig. 5 a Break water piers using natural boulders across the waterfront of Sykea village do seem to have reduced the retrogradation phenomenon but an average of 20 m of coastal zone has been lost in a 72-year period. **b** Several measures and constructions along the Xilokastro waterfront have slowed down the coastal erosion that reached the rate of 0.66 m/year for the study time period. **c** The highest rates of retrogradation were calculated along the Kamari beachfront where serious damages are expected the next few years, as no serious measures have been taken for the coastal conservation. See Fig. 1 for the locations of the photographs

Sythas estuary (transects 64–65) and was completed during 1987, altering violently the coastal zone balance and this is the reason why this small segment measurements were not included in the coastal zone analysis. The protection measures along the Xilokastro waterfront seem to have significantly reduced the shoreline retreat which was calculated at 0.26 ± 0.04 m/ year since 1945, even if there are transects with no human interference, where the beach width has been retrograded by more than 50 m yielding an erosion rate of 0.66 ± 0.03 m/year (transect 49). During the last three decades the shoreline matches the construction boundaries and therefore the wave eroding dynamics affect mainly the retaining wall causing serious damage. Two locations for the conduction of submarine profiles were selected along this segment; one along the transect 50 at its easternmost boundary (profile D), facing ENE and the second at its westernmost profile along transect 60 (profile E), facing NNE. Both profiles show relatively steep subaqueous relief, with overall slopes of 25% and 24%, respectively. More specifically, profile D can be divided into two segments of significantly different slopes; the first one up to the depth of 5 m, about 50 m from the shoreline, with a slope of about 10% and the second one, from the depth of 5 m to the depth of 20 m, about 90 m from the shoreline, with a slope of 37%. This difference in slopes could be justified due to the orientation of the shoreline at the specific area, which is of NNW-SSE direction, in relation to the overall orientation of the broader area (NW-SE). Comparing the contemporary seabed morphology with the one from 2010 (Fig. 4), we conclude that the two segments of different slopes are also present at the older profile, with the exception of a rather important advance of the seabed morphology after the depth of 5 m, reaching an expansion of about 25 m at the depth of −10 m during the last 7 years. This expansion, given the fact that the sediment supply from Sythas river has remained stable, could be caused due to submarine mass movements which potentially have affected the coastal zone width.

Profile E presents similar seabed morphology and slope with profile D, with the exception of the area of depths up to −8 m, in which for the profile E covers a length of about 20 m further than on profile D. The comparison with the profile conducted during 2010 (Fig. 4) presents similar characteristics with the one of profile D and can be ascribed to the same factors as in profile D.

Westward of the yacht marina we observe the highest progradation values (0.26 ± 0.04 m/year at transect 66), where sediment deposition led to beach accretion for more than 20 m clearly due to the jetty construction. For the next 2 km (transects 67–86) heading west, the coastal zone could be segmented in several parts where there are no erosion protection measures intercalated by segments where large piers using natural boulders have been constructed for reducing the erosive ability of the incoming waves. The average erosion rate for the entire segment (SG-V, Fig. 3) is calculated at 0.09 ± 0.03 m/

year since 1945, but there are locations with high retreat rates $(0.26 \pm 0.04$ m/year at transect 73, placed between two piers) coexisting with locations showing stable shoreline or even low progradation rates when the transects are sketched normally to breakwater piers. The seabed morphology of profile F (in transect 70) was conducted at a segment without any manmade intervention. It presents the smoothest slope of 4% up to the depth of -10 and a small steepening up to the depth of -20 m at 310 m away from the shoreline, with a slope of 14%. The comparison of this profile with the one conducted during 2010 (Fig. 4) presents no significant alterations in the seabed for the last 7 years.

The most stable segment without erosion phenomena is found at the next 0.5 km westwards (SG-VI, Fig. 3). It seems that the breakwater piers have preserved the width of the coastal zone and in some cases progradation was observed with relatively high rates $(0.21 \pm 0.05$ m/year at transect 90). This narrow segment is acting as an intercalation within two larger segments with erosional phenomena taking place.

The last almost 3-km long segment (SG-VII, Fig. 3) is characterized by the continuous presence of measures and constructions for the preservation of the coastal zone. The entire waterfront is covered by dense residential land and it seems that in many cases the land owners decided to act autonomously and with anarchy regarding the prevention of their properties from serious damage without any scientific method. The measures include boulder placements, corral constructions or even concrete mass droppings along the coastline aiming to keep the wave breaking far from their houses as it should be highlighted that in most cases, the building activity has been expanded on the coastal zone or even on the seaside (Fig. 5c). Apparently, the effectiveness of those measures which have been taken without the approval of the local authorities, is rather questionable as the average erosion rate along this 3-km long segment is estimated at 0.28 ± 0.03 m/year, whilst the highest rate is calculated at 0.67 ± 0.07 m/year (transects 115–116) for the entire study period. During this time period the width of the coastal zone has been significantly reduced by more than 25 m. The submarine profile F that was conducted at the location of transect 98 (with erosion rate near the average value 0.27 ± 0.05 m/year) indicates a rather smooth sea bottom relief, with a slope of 7%, without any signs of geodynamic phenomena that would affect the retrogradation of this segment. Therefore, the reasons for the high rates of erosion at this location should be present mostly due to the human intervention and intrusion on the coastal environment and less to physical processes.

Conclusions

The described methodology introduces a simple but very convenient way of combining a dataset containing all the available shoreline traces throughout a given time period, in order to quantify its displacement rate for certain segments and therefore evaluate the risk or vulnerability of a coastal zone. We suggest that all kinds of remote sensing data (with similar spatial resolution) could be included in this change detection procedure and the objective difficulty should be how far back in time one could find reliable datasets and hence increase the reliability of the methodology. The most labored issue would be to make all the collected datasets free from distortions and consequently comparable to each other, combine them in a Geographic Information System platform and finally determine and quantify the shoreline displacement rate and especially the erosion rate at certain segments.

By employing the methodology described above, we collected, processed and analyzed historic analog panchromatic aerial images, recent digital high-resolution multi-spectral satellite images along with contemporary aerial images acquired by a low cost UAS covering a time period of 72 years with eight remote sensing datasets. The shoreline location change rates that we calculated were not homogeneous along the full length of the coastal area of interest but the methodology results provided useful information for segmenting it in more uniform zones and conducting submarine profiles. In some cases, the subaqueous relief showed formations compatible with instabilities that may have affected the nearshore part of the coastal zone, but there were also cases that even the sea bottom is smooth and free of mass movement phenomena, the calculated erosion rates are extremely high. Specifically, the average value of the rate of receding is 0.18 ± 0.03 m/year, while extreme values of order 0.70 ± 0.03 m/year were also observed, narrowing the beach by about 50 m and increasing the riskiness of specific locations, despite the fact that several kinds of protection measures have been taken for many years in order to preserve the coastal zone.

References

Agisoft (2016) Agisoft Photoscan user manual: professional edition (v.1.2), Retrieved 23/7/2016, http://www.agisoft.com/pdf/photoscan-pro_1_2_en.pdf

Albini P, Rovida A, Scotti O, Lyon-Caen H (2017) Large eighteenth–nineteenth century earthquakes in western gulf of Corinth with reappraised size and location. Bull Seismol Soc Am 107:1663–1687. https://doi.org/10.1785/0120160181

Alhin KA, Niemeyer I (2009) Coastal monitoring using remote sensing and geoinformation systems: Estimation of erosion and accretion rates along Gaza coastline. In: Geoscience and Remote Sensing Symposium, 2009 I.E. International IGARSS 2009, 12–17

July 2009. pp IV-29-IV-32. doi:https://doi.org/10.1109/igarss.2009.5417605

Anthoff D, Nicholls RJ, Tol RSJ (2010) The economic impact of substantial sea-level rise. Mitig Adapt Strateg Glob Chang 15:321–335. https://doi.org/10.1007/s11027-010-9220-7

Bell RE, McNeill LC, Bull JM, Henstock TJ, Collier REL, Leeder MR (2009) Fault architecture, basin structure and evolution of the Gulf of Corinth rift, central Greece. Basin Res 21:824–855. https://doi.org/10.1111/j.1365-2117.2009.00401.x

Boak EH, Turner IL (2005) Shoreline definition and detection: a review. J Coast Res 21:688–703. https://doi.org/10.2112/03-0071.1

Chaaban F, Darwishe H, Battiau-Queney Y, Louche B, Masson E, Khattabi JE, Carlier E (2012) Using ArcGIS® Modelbuilder and aerial photographs to measure coastline retreat and advance: North of France. J Coast Res 285:1567–1579. https://doi.org/10.2112/jcoastres-d-11-00054.1

Charalampakis M, Lykousis V, Sakellariou D, Papatheodorou G, Ferentinos G (2014) The tectono-sedimentary evolution of the Lechaion Gulf, the south eastern branch of the Corinth graben, Greece. Mar Geol 351:58–75. https://doi.org/10.1016/j.margeo.2014.03.014

Church JA et al (2013) Climate change 2013: the physical science basis. Contribution of Working Group I to the Fifth Assessment Report of the Intergovernmental Panel on Climate Change Sea level change: 1137–1216

Costanza R et al (1997) The value of the world's ecosystem services and natural capital. Nature 387:253–260. https://doi.org/10.1038/387253a0

De Pippo T, Donadio C, Pennetta M, Petrosino C, Terlizzi F, Valente A (2008) Coastal hazard assessment and mapping in northern Campania, Italy. Geomorphology 97:451–466. https://doi.org/10.1016/j.geomorph.2007.08.015

Evans E et al (2004) Foresight future flooding, scientific summary, volume I: future risks and their drivers. Office of Science and Technology, London

Evelpidou N, Pirazzoli PA, Saliège JF, Vassilopoulos A (2011) Submerged notches and doline sediments as evidence for Holocene subsidence. Continental Shelf Research 31:1273–1281. https://doi.org/10.1016/j.csr.2011.05.002

Fonstad M, Dietrich J, Courville B, Jensen J, Carbonneau P (2013) Topographic structure from motion: a new development in photogrammetric measurement. Earth Surf Process Landf 38:421–430. https://doi.org/10.1002/esp.3366

Gens R (2010) Remote sensing of coastlines: detection, extraction and monitoring. Int J Remote Sens 31(7):1819–1836. https://doi.org/10.1080/01431160902926673

Hellenic Navy Hydrographic Service (2015) Sea level statistics from the Greek tide gauge network, publication of Hellenic navy hydrographic Service, Athens, 107 p

Hollenstein C, Muller MD, Geiger A, Kahle HG (2008) Crustal motion and deformation in Greece from a decade of GPS measurements, 1993-2003. Tectonophysics 449:17–40. https://doi.org/10.1016/j.tecto.2007.12.006

Kloehn KK, Beechie TJ, Morley SA, Coe HJ, Duda JJ (2008) Influence of dams on river-floodplain dynamics in the Elwha River, Washington. Northwest Sci 82:224–235. https://doi.org/10.3955/0029-344x-82.s.i.224

Lykousis V et al (2007) Sediment failure processes in active grabens: the western gulf of Corinth (Greece). In: Lykousis V, Sakellariou D, Locat J (eds) Submarine mass movements and their consequences: 3rd international symposium. Springer Netherlands, Dordrecht, pp 297–305. https://doi.org/10.1007/978-1-4020-6512-5_31

Malthus TJ, Mumby PJ (2003) Remote sensing of the coastal zone: an overview and priorities for future research. Int J Remote Sens 24: 2805–2815. https://doi.org/10.1080/0143116031000066954

Mancini F, Dubbini M, Gattelli M, Stecchi F, Fabbri S, Gabbianelli G (2013) Using unmanned aerial vehicles (UAV) for high-resolution reconstruction of topography: the structure from motion approach on coastal environments. Remote Sens 5:6880–6898. https://doi.org/10.3390/rs5126880

McClusky S et al (2000) Global positioning system constraints on plate kinematics and dynamic in the eastern Mediterranean and Caucasus. J Geophys Res 105:5695–5719. https://doi.org/10.1029/1999JB900351

Moore LJ (2000) Shoreline Mapping Techniques. J Coast Res 16:111–124. https://doi.org/10.2307/4300016

Mugnier C (2002) Grids and Datums: the Hellenic Republic. Photogramm Eng Remote Sens 68:1237–1238

Nicholls RJ, Hoozemans FMJ (1996) The Mediterranean: vulnerability to coastal implications of climate change. Ocean & Coastal Management 31(2-3):105–132. https://doi.org/10.1016/S0964-5691(96)00037-3

Nomikou et al (2011) Swath bathymetry and morphological slope analysis of the Corinth gulf. In: Grützner C, Fernández Steeger T, Papanikolaou I, Reicherter K, Silva PG, Pérez-López R, Vött a (eds) 2nd INQUA-IGCP-567 international workshop on active tectonics, Earthquake Geology, Archaeology and Engineering, Corinth, 2011. pp 46–49

Padwick C, Pacifici F, Smallwood S (2010) WorldView-2 pan-sharpening. In: ASPRS 2010 Annual Conference, San Diego

Sakellariou D et al (2007) Faulting, seismic-stratigraphic architecture and late quaternary evolution of the Gulf of Alkyonides Basin–East Gulf of Corinth, Central Greece. Basin Res 19:273–295. https://doi.org/10.1111/j.1365-2117.2007.00322.x

Thieler E, Himmelstoss E, Zichichi J, Ergul A (2009) Digital shoreline analysis system (DSAS) version 4.3-an ArcGIS extension for calculating shoreline change. Vol 2008-1278. U.S. Geological Survey

Valaouris A, Poulos S, Petrakis S, Alexandrakis G, Vassilakis E, Ghionis G (2014) Processes affecting recent and future evolution of the Xylokastro beach zone (semi-enclosed Gulf of Corinth, Greece). Global NEST J 16:773–786

Van Rijn LC (1998) Principles of coastal morphology. Aqua publications, Amsterdam

Van Zuidam R, Van Zuidam-Cancelado F (1979) terrain analysis and classification using aerial photographs: a geomorphological approach. International Institute for Aerial Survey and Earth Sciences (ITC)

Vassilakis E (2010) Remote sensing of environmental change in the Antirio deltaic fan region, western Greece. Remote Sens 2:2547–2560. https://doi.org/10.3390/rs2112547

Vassilakis E, Papadopoulou-Vrynioti K (2014) Quantification of deltaic coastal zone change based on multi-temporal high resolution earth observation techniques. ISPRS Int J Geo-Inf 3(1):18–28. https://doi.org/10.3390/ijgi3010018

Vassilakis E, Skourtsos E, Kranis H (2007) Combination of morphometric indices as a method for the quantification of neotectonic evolution in active areas. In: 16th DRT Conference, Milan, Rend. Soc. Geol. It., p 214

Vassilakis E, Royden L, Papanikolaou D (2011) Kinematic links between subduction along the Hellenic trench and extension in the Gulf of Corinth, Greece: a multidisciplinary analysis. Earth Planet Sci Lett 303:108–120. https://doi.org/10.1016/j.epsl.2010.12.054

Westoby MJ, Brasington J, Glasser NF, Hambrey MJ, Reynolds JM (2012) 'Structure-from-motion' photogrammetry: a low-cost, effective tool for geoscience applications. Geomorphology 179:300–314. https://doi.org/10.1016/j.geomorph.2012.08.021